Supporting Information

Metamaterials with in-situ tunable bending properties

Miao Yu[1,2], *Xin Fang**[1,2], *Dianlong Yu**[1,2]

1. National Key Laboratory of Equipment State Sensing and Smart Support, National University of Defense Technology, Changsha 410073, People's Republic of China
2. College of Intelligence Science and Technology, National University of Defense Technology, Changsha 410073, People's Republic of China

E-mail: xinfangdr@sina.com(X. Fang); dianlongyu@vip.sina.com(D. L. Yu)

Files:

Section S1. The longitudinal stiffness of the planetary gear assemblies in Sample 1 and 2

The longitudinal stiffness of the planetary gear assemblies can be obtained by finite element simulation. As shown in the left part in **Figure S1(a)**, the longitudinal stiffness (k_y) is defined as the tension/compression stiffness at the location where force F_y is applied. The finite element model of the planetary gear assembly is shown in the right part of **Figure S1(a)**. In this model, the sun gear and planetary gears are collectively simplified into a single cross-shaped structure, which is assigned a bonded contact condition with the ring gear. For the simulation, the Young's modulus of the ring gear is defined as 2 GPa. To incorporate the mechanical influence of the planetary gears, the Young's modulus of the central cross-shaped structure is specified as 0.3 GPa. The boundary conditions applied in the model include a fixed support at the lower end of the assembly and a prescribed force at the upper end, from which the corresponding deformation is obtained. Accordingly, the stiffness of the planetary gear assembly is determined as the ratio of the applied force to the resulting deformation.

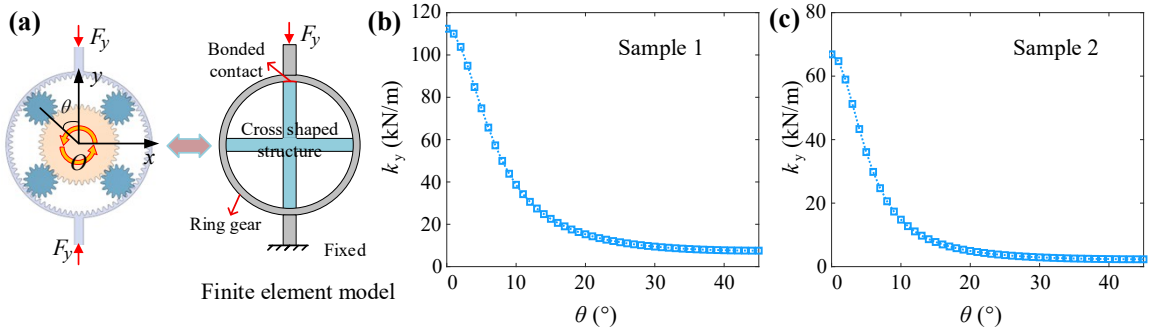

Figure S1. Finite element simulation results about longitudinal stiffness of the planetary gear assemblies in Sample 1 and 2 under different θ: (**a**) The longitudinal stiffness of the planetary gear assemblies. (**b**) Variation of the longitudinal stiffness with θ for Sample 1. (**c**) Variation of the longitudinal stiffness with θ for Sample 2.

Based on finite element model we can get the longitudinal stiffness of the planetary gear assemblies in Sample 1 and 2, as shown in **Figure S1(b,c)**. The results show that the longitudinal stiffness varies continuously with the angle θ and it can be tuned from 7.5 kN/m to 112.5 kN/m for Sample 1, from 2.3 kN/m to 66.9 kN/m for Sample 2.

We can see that the variation in the longitudinal stiffness of the planetary gear assemblies concentrate mainly in the first half of the angle change, this occurs due to a fundamental shift in the load-bearing mechanism. At the initial position (small rotation angle θ), the system's high longitudinal stiffness is predominantly provided by the positive pressure stiffness generated by the planet gears and the sun gear. This configuration offers substantial

resistance to longitudinal deformation. As the planet gears begin to rotate from this position, they gradually disengage from the primary load-bearing contact points. This disengagement leads to a rapid and significant drop in the contribution from the planet gears and the sun gear, causing a sharp decrease in the overall system stiffness. Once the planet gears have largely disengaged from the initial high-stiffness state, the longitudinal stiffness is then primarily sustained by the ring gear. Further rotation mainly alters the effective length of the ring gear's teeth. This results in a much slower and more gradual decline in stiffness during the latter half of the angle change.

Section S2. Controlled experiment for the meta-beam.

Table S1. Structural parameters of meta-beam Sample 1, Comparison 1 to 3 and Sample 2

	b	*h*	*l*	*r*	ring gear's radius	ring gear's thickness
Sample 1	30 mm	3 mm	0.05 m	20 mm	15 mm	1 mm
Comparison 1	30 mm	3 mm	0.05 m	20 mm	15 mm	0.5 mm
Comparison 2	30 mm	1 mm	0.05 m	20 mm	15 mm	1 mm
Comparison 3	30 mm	3 mm	0.05 m	30 mm	15 mm	1 mm
Sample 2	30 mm	1 mm	0.05 m	30 mm	15 mm	0.5 mm

To verify that the greater variation range of k_B in Sample 2 compared to Sample 1 results from its thinner center beam (h = 1 mm), longer pillars (r = 30 mm), and larger variation in the longitudinal stiffness of the planetary gear assemblies, a controlled experiment is performed using three comparative samples (Comparison 1-3). Comparison 1 exhibits a larger variation in longitudinal stiffness of the planetary gear assemblies than Sample 1; Comparison 2 adopts a thinner center beam (h = 1 mm); and Comparison 3 incorporates longer pillars (r = 30 mm). Their structural parameters are listed in Table S1. All samples are fabricated from resin via 3D printing with material parameters identical to those of Samples 1 and 2. The three-point bending test is employed to measure the maximum and minimum bending stiffness as well as the stiffness variation ratio for each comparative sample, and the results are summarized in Table S2. The experiments confirm that modifying any single parameter(a thinner center beam, longer pillars, or a greater variation in longitudinal stiffness

of the planetary gear assemblies) can effectively increases the stiffness variation range relative to Sample 1, thereby supporting the above conclusion.

Table S2. Min k_B, max k_B and R_B of meta-beam Sample 1, Comparison 1 to 3 and Sample 2

	Min k_B (N/m)	Max k_B (N/m)	R_B
Sample 1	397	2178	5.5
Comparison 1	237.8	2125.1	8.9
Comparison 2	113.4	1064.8	9.4
Comparison 3	520.8	3189.3	6.1
Sample 2	108.2	1958	18.1

Section S3. Finite element analysis about influences of unit density on the global tunable range of meta-beam with fixed total length

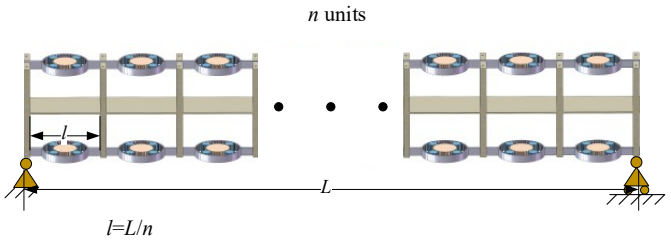

Figure S2. Finite element model of meta-beam with fixed total length

The variation range of the bending stiffness for the meta-beam can be influenced by the unit density. So we investigate the influence of unit number on bending stiffness modulation in fixed total length meta-beams through finite element analysis (FEA). As shown in **Figure S2**, we establish a finite element model with fixed total length of L and simply supported boundary. The number of units n defines the unit length by $l=L/n$. Based on the structural parameters, the variation range of bending stiffness for Sample 1 and Sample 2 under different values of n can be determined.

In finite element simulation the total length of meta-beam is 0.4 m for both Sample 1 and Sample 2. The longitudinal stiffness of the planetary gear assemblies in Sample 1 is set from

7.5 kN/m to 112.5 kN/m for Sample 1 and from 2.3 kN/m to 66.9 kN/m for Sample 2. This stiffness remains constant and does not vary with n. The bending stiffness is obtained through three-points bending model by applying a force at the middle point of meta-beam. The tunable range of bending stiffness is $R_B = \max(k_B)/\min(k_B)$.

When the number of cells n is small, the structure is insufficiently periodic to be considered a homogeneous metastructure. Under these conditions, the homogenization assumptions do not yet apply. Instead, the tunable stiffness capability initially improves as n increases because the structure begins to exhibit more consistent periodic behavior.

As n continues to increase, the meta-beam becomes sufficiently periodic for homogenization theory to become applicable. In this regime, the finite-element results gradually converge toward the homogenization predictions. According to the homogenization model, further reduction in l (increase in n) leads to a decrease in the achievable stiffness variation—a trend that is clearly reflected in the simulation results for larger n.

These results highlight that the unit-cell size should be neither too large nor too small. Excessively large cells lead to non-periodic behavior and reduced tunability, while excessively small cells weaken the stiffness variation while increasing structural complexity. An intermediate cell size therefore offers the best compromise between performance and practical feasibility.

Section S4. Frequency responses of the meta-beam vary with θ: experimental and simulation results

The frequency responses of Samples 1 and 2 under varying rotation angle θ of the sun gears are shown in **Figure S3**.

For Sample 1, experimental results in **Figure S3(a)** indicate that the first resonant frequency increases from 21.25 Hz to 45.31 Hz, the second from 111.9 Hz to 173.4 Hz, and the third from 277.2 Hz to 357.5 Hz. Corresponding FEM simulations in **Figure S3(b)** show consistent trends and comparable values, with the first resonant frequency rising from 20 Hz to 44 Hz, the second from 115 Hz to 177 Hz, and the third from 295 Hz to 381 Hz.

For Sample 2, experimental data in **Figure S3(c)** demonstrate that the first resonant frequency increases from 7.813 Hz to 31.25 Hz, the second from 33.44 Hz to 97.5 Hz, the third from 72.5 Hz to 174.1 Hz, and the fourth from 103.8 Hz to 235.9 Hz. Similarly, FEM results in **Figure S3(d)** exhibit closely matching trends, with the first resonant frequency

increasing from 8 Hz to 30 Hz, the second from 40 Hz to 94 Hz, the third from 92 Hz to 156 Hz, and the fourth from 132 Hz to 200 Hz.

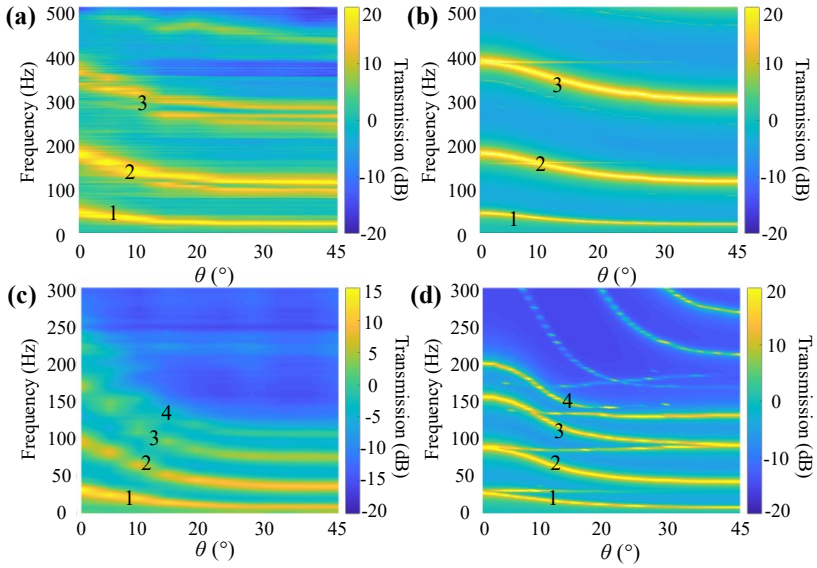

Figure S3. Frequency response of meta-beam vary with θ obtained by Experiment and FE simulation. **(a)** Experimental results of Sample 1. **(b)** Simulation results of Sample 1. **(c)** Experimental results of Sample 2. **(d)** Simulation results of Sample 2.

As shown in **Figure S4**, , the finite element simulation reveals the first four resonance modes of the meta-beam. The results confirm that these modes correspond to fundamental bending resonances, rather than higher-order or parasitic modes.

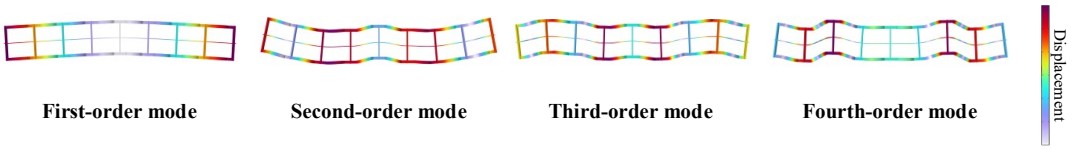

Figure S4. The first four resonance modes of the meta-beam.

Section S5. Modal shape for Meta-plate I, II and III vary with θ obtained by FE simulation.

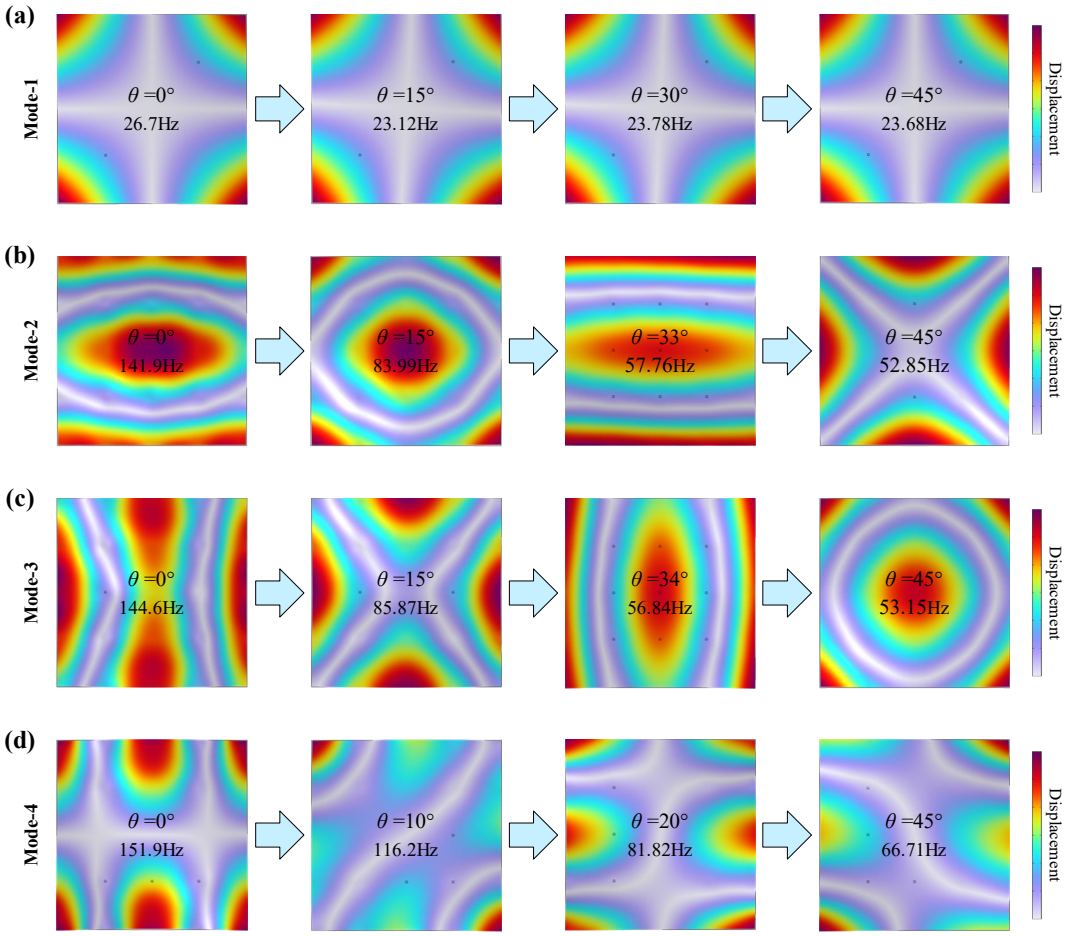

Figure S5 Variation of modal shapes with sun gear rotation angle θ for Meta-plate I. **(a)** Mode-1. **(b)** Mode-2. **(c)** Mode-3. **(d)** Mode-4.

The tunable frequency response of Meta-plate is realized with synchronously controlled planetary gear assemblies. The frequency curves may intersect when changing the rotation angle. Thus, using the term "order" for modal shape definition is ambiguous. We define them as mode-1 (first-order mode when θ = 0°) to mode-4 (fourth-order mode when θ= 0°). For Meta-plate I the frequency of mode-1 is non-sensitivity to θ, whereas modes 2~4 show great frequency variation while rotation angle θ from 0 to 15°: The mode-2 frequency adjusts from 141.9 Hz to 52.85 Hz, the tmode-3 from 144.6 Hz to 53.15 Hz, and the mode-4 from 151.9 Hz to 66.71 Hz.

The variation processes of the modal shapes of Meta-plate I are illustrated in **Figure S5**. Detailed modal shape transformation are provided in Supplementary Video S1. When changing θ, the first-order mode frequency remains invariant because its modal shape primarily induces large deformation in the diagonal directions, but the diagonal fibers are not

connected by the planetary gear assemblies, thus preventing control over this mode. In contrast, the second to fourth-order modes exhibit significant changes because their modal shapes induce large deformation in x and y axes, just aligning with the designed coupling directions.

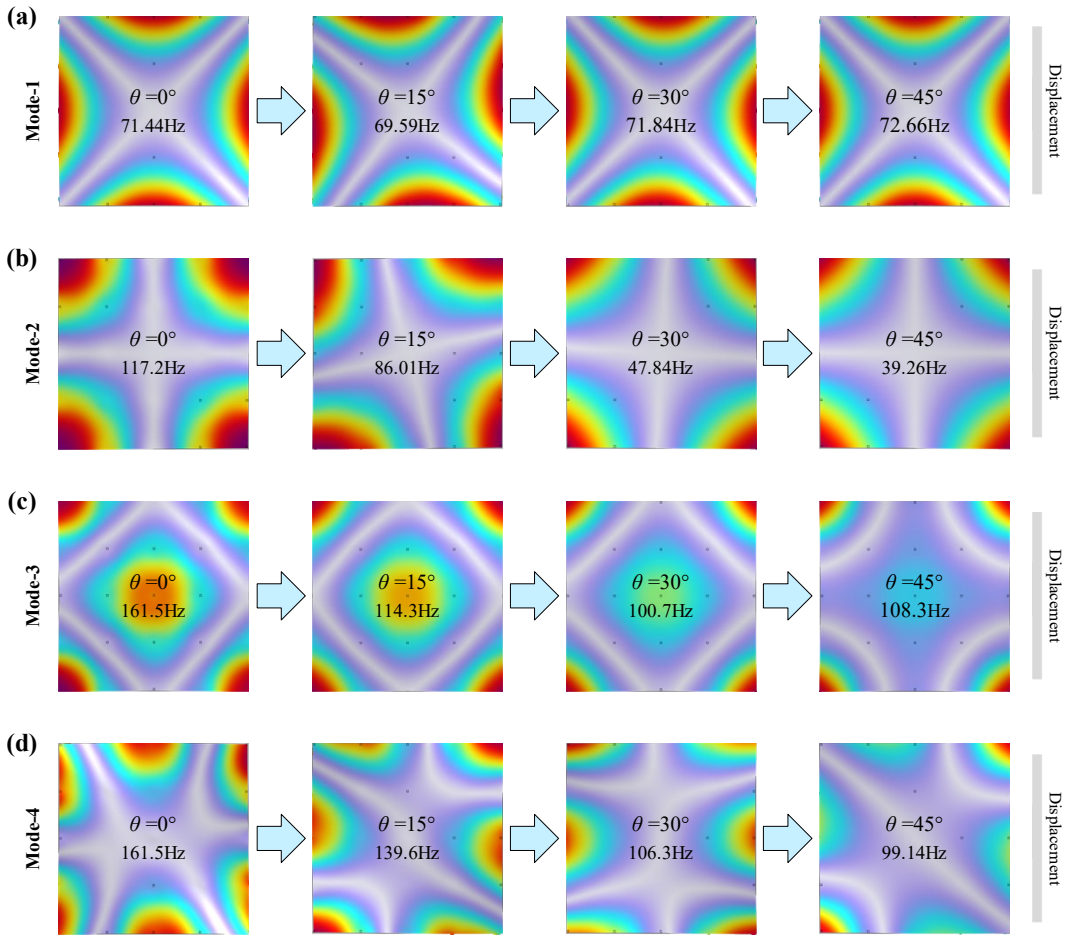

Figure S6 Variation of modal shapes with sun gear rotation angle θ for Meta-plate II. **(a)** Mode-1. **(b)** Mode-2. **(c)** Mode-3. **(d)** Mode-4.

Including the modal frequencies, rotating all local planetary gear assemblies will change the global shapes of modes 2~4. Some modes may switch be changing the rotation angle. For example, the shapes for θ = 15° under 83.99 Hz and θ = 45° under 53.15 Hz, θ = 45° under 52.85 Hz and θ = 15° under 85.87 Hz, are approximately same. Changing the modal shapes is also significant in practice because it will change the vibration energy distribution for vibration protection. For example, if we put an important instrument at the center of the meta-plate and want to suppress its vibration, changing modal shape can make it be silent under different frequencies. We term this phenomenon as active modal reshaping. This discovery is benefit for controlling the response for vibration suppression purposes.

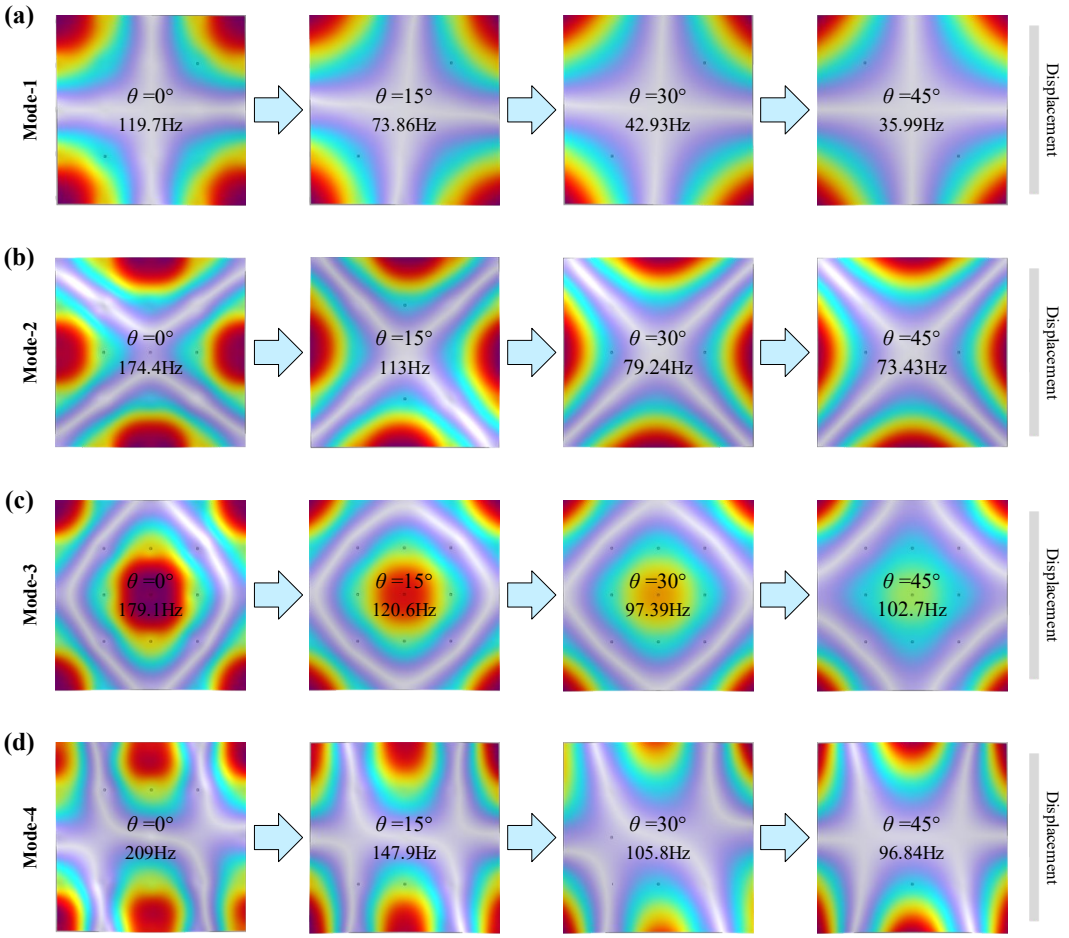

Figure S7 Variation of modal shapes with sun gear rotation angle θ for Meta-plate III. **(a)** Mode-1. **(b)** Mode-2. **(c)** Mode-3. **(d)** Mode-4.

For Meta-plate II, the frequency of mode-1 is nearly invariant near 71Hz, because its mode shape induces much smaller deformation in the diagonal directions than the *x*-*y* orthogonal directions. The remaining three modes' frequencies are broadly tunable because their shapes induce large deformation in diagonal directions: The resonant frequency for mode-2 can be tuned from 117.2 Hz to 39.26 Hz, the mode-3 from 161.5 Hz to 99.59 Hz, and the mode-4 from 161.6 Hz to 99.14 Hz. Compared with Meta-plate I, Meta-plate II exhibits comparable tuning capability for the second to fourth resonant frequencies. However, the mode reshaping is not significant for these modes in meta-pate II, as illustrated in **Figure S6**. Detailed modal shape transformation are provided in Supplementary Video S2.

For Meta-plate II, we can observe the phenomenon that the mode 2 appears to cross mode 1 after approximately 20 degrees, this is due to the directional dependence of bending stiffness in Meta-plate II. As shown in the Supplementary Figure S6: Mode 1 is governed by the bending stiffness in the *x* and *y* directions, which remains unchanged in this design. Mode

2 is dominated by the in-plane shear (*xy* direction) bending stiffness, which decreases with gear rotation. Consequently, as rotation proceeds beyond approximately 20 degrees, the frequency of Mode 2 decreases below that of Mode 1, resulting in the observed crossing.

Compared to meta-plates I and II, Meta-plate III shows stronger ability in regulating resonance frequency, even for mode-1. The resonant frequency for mode-1 ranges from 119.7 Hz to 35.99 Hz, the mode-2 from 174.4 Hz to 73.43 Hz, the mode-3 from 179.1 Hz to 95.58 Hz, and the mode-4 from 209 Hz to 96.84 Hz. Crucially, the modal shapes at different rotation angles remain almost unchanged, as shown in **Figure S7**. Therefore, the mode reshaping depends on the connections in unit cells. Detailed modal shape transformation are provided in Supplementary Video S3.

Section S6. Frequency responses of the meta-plate vary with θ: experimental and simulation results

To validate the tunable vibration characteristics of the meta-plate, we fabricate a 4×4 units array of Meta-plate III and experimentally measure its vibration response under varying planetary gear rotation angles. The plate body and planetary gear systems are 3D-printed from resin, while steel pillars are incorporated. Vibration testing employs a midpoint excitation configuration: the plate's center point is rigidly fixed to an exciter while maintaining free boundaries.

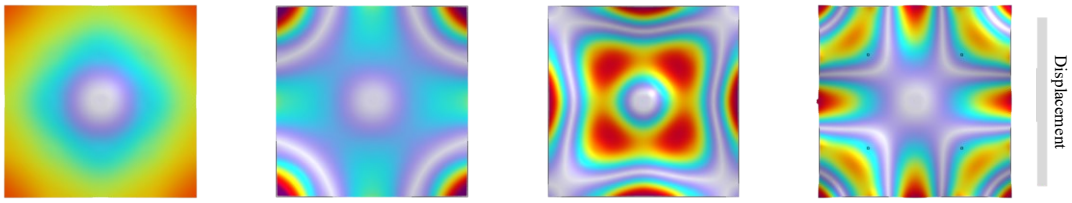

Figure S8 Modal shapes of Mode-1 to Mode-4 for Meta-plate III under midpoint excitation.

Finite element modeling under experimental equivalent conditions revealed the plate's modal shapes, as shown in **Figure S8**. Under midpoint excitation, these mode shapes differ from the free-vibration modes in **Figure S7**. Similarly, modal shapes under midpoint excitation do not change with θ though frequencies of Mode-1 to Mode-4 change with θ.

For Meta-plate III, experimental results in **Figure S9(a)** indicate that the frequency of Mode-1 increases from 37.34 Hz to 52.97 Hz, the Mode-2 from 133.8 Hz to 206.1 Hz, the third from 210.7 Hz to 300.9 Hz and the Mode-4 from 263.9 Hz to 410.7 Hz. Corresponding FEM simulations in **Figure S9(b)** show consistent trends and comparable values, with the Mode-1 increases from 38 Hz to 60 Hz Hz, the Mode-2 from 118 Hz to 220 Hz Hz, the third from 192 Hz to 312 Hz Hz and the Mode-4 from 240 Hz to 382 Hz.

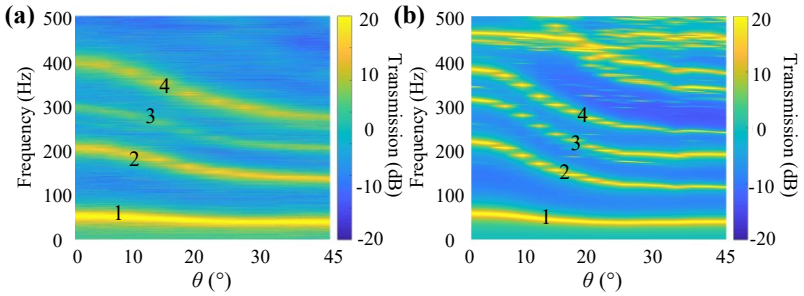

Figure S9. Frequency response of Meta-plate III vary with θ obtained by Experiment and FE simulation. **(a)** Experimental results. **(b)** Simulation results.

Section S7. Vibration mode analysis of meta-beam

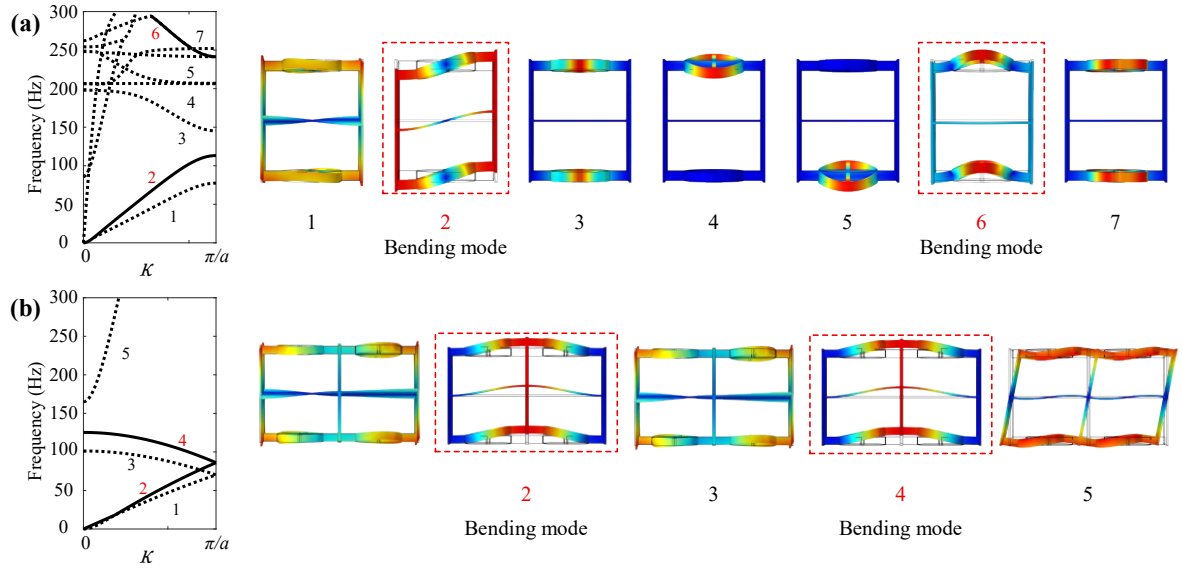

Figure S10. Vibration mode analysis of meta-beam. **(a)** Vibration mode of mass-based meta-beam when θ=0°. **(b)** Vibration mode of stiffness-difference-based meta-beam when θ_L-θ_R=0°-0°.

The first approach to inducing a band gap involves increasing the mass of the sun gear in the units which is referred to as a mass-based meta-beam. As an example, we calculate its band structure at θ = 0° by applying Bloch-Floquet periodic boundary conditions, as

illustrated in **Figure S10(a)**. The corresponding modal shapes are also obtained. Since this study focuses on the propagation of bending waves, we distinguish bending-wave branches by solid lines and other modes by dashed lines in the band structure. Based on the modal shapes (right panel of **Figure S10(a)**), it can be determined that Curve 2 and Curve 6 (left panel of **Figure S10(a)**) correspond to bending waves, while the remaining curves represent waves of other modes. A frequency range where bending waves cannot propagate but other modes can is termed a bending wave attenuation band. In contrast, a frequency range in which no waves of any mode can propagate is defined as a complete band gap (also referred to simply as a band gap).

Another method for inducing a band gap is to combine two units into a larger metacell, where the left and right units are independently controlled by their respective rotation angles, θ_L and θ_R. A band gap is induced when $\theta_L \neq \theta_R$ as this creates a stiffness difference between the two units. We calculated the band structure for the case of θ_L-θ_R=0°-0° and obtained the corresponding modal shapes, as shown in **Figure S10(b)**. Analysis of these modal shapes (right panel of **Figure S10(b)**) confirms that Curves 2 and 4 (left panel of **Figure S10(b)**) represent bending waves, while the remaining curves correspond to other wave modes.

Section S8. Detailed parameters and materials of meta-beam Sample 3 to 6

In order to study the bending stiffness and its variation range of the meta-beams with structural parameters beyond those of Sample 1 and Sample 2, we conduct finite element modeling for Samples 3 to 6 (as listed in **Table S3**) and calculate their bending stiffness under three-point bending.

Sample 3 and Sample 4 are made primarily of resin, with the pillar made of steel; Sample 5 is primarily aluminum alloy, also with steel pillars; and Sample 6 is fabricated entirely from steel.

Table S3. Structural parameters of meta-beam Sample 3 to Sample 6

	b	*h*	*l*	*r*	ring gear's radius	ring gear's thickness
Sample 3	30 mm	1 mm	0.05 m	30 mm	20 mm	0.5 mm
Sample 4	30 mm	1 mm	0.05 m	30 mm	20 mm	0.3 mm
Sample 5	30 mm	1 mm	0.05 m	30 mm	20 mm	0.5 mm
Sample 6	30 mm	1 mm	0.05 m	30 mm	20 mm	0.5 mm

The finite element results indicate that the bending stiffness of Sample 3 can be adjusted from 55.89 N/m to 1339 N/m, representing a 23.9 times variation. The bending stiffness of Sample 4 can be tuned from 26.39 N/m to 1278 N/m, corresponding to a 47.5 times multiple. Sample 5 exhibits a stiffness range from 2007 N/m to 41,070 N/m, achieving a 20.5 times increase, while Sample 6 can be adjusted from 5543 N/m to 97,150 N/m, resulting in a 17.5 times multiplication.